

A Common Architecture for Human and Artificial Cognition Explains Brain Activity Across Domains

Authors: Andrea Stocco^{1*}, Zoe Steine-Hanson^{2,†}, Natalie Koh^{1‡}, John E. Laird³, Christian J. Lebiere⁴, and Paul S. Rosenbloom⁵

Affiliations:

¹University of Washington, Seattle, WA 98195.

²Oregon State University, Corvallis, OR 97331.

³University of Michigan, Ann Arbor, MI 48109.

⁴Carnegie Mellon University, Pittsburgh, PA 15213.

⁵University of Southern California, Los Angeles, CA 90089.

[†]Now at University of Washington, Seattle, WA 98195.

[‡]Now at Northwestern University, Chicago, IL 60208.

*Correspondence to: stocco@uw.edu.

Abstract: The Common Model of Cognition (CMC) is a consensus architecture for human and human-like artificial cognition. We hypothesized that, because of its generality, the CMC could be a candidate model of the large-scale functional architecture of the human brain. To this end, we analyzed neuroimaging from $N=200$ participants across seven tasks that cover the broad range of cognitive domains. The CMC framework was translated into a model of neural connectivity between brain regions homologous to CMC components. After the model was implemented and fitted using Dynamic Causal Modeling, its performance was compared against four alternative large-scale brain architectures that had been previously proposed in the field of neuroscience. The results show that the CMC outperforms the other four architectures within and across all domains. These findings suggest that a common, functional computational blueprint for human-like intelligence also captures the neural architecture that underpins human cognition.

One Sentence Summary: A consensus computational architecture for modeling both human and human-like intelligence also best explains human neuroimaging activity across cognitive domains.

Main Text

The fundamental organizational principle of a complex system is often referred to as its “architecture,” and represents an important conceptual tool to make sense of the relationship between a system’s function and structure. For instance, the von Neumann architecture describes the organizing principle of modern digital computers; it can be used both to describe a computer at a functional level of abstraction (ignoring the specific wiring of its motherboard) and, conversely, to conduct diagnostics on an exceedingly complicated piece of hardware (properly identifying the components and pathways on a motherboard and the function of their wiring).

The stunning complexity of the human brain has inspired a search for a similar “brain architecture” that, akin to von Neumann’s, could relate its components to its functional properties. Succeeding in this quest would lead to a more fundamental understanding of brain function and dysfunction and, possibly, to new principles that could further the development of artificial intelligence (1).

Most attempts in this direction have been “bottom-up,” that is, driven by the application of dimensionality-reduction and machine-learning methods to large amounts of connectivity data, with the goal of identifying clusters of functionally connected areas (2–4). Although these models can be used to predict task-related activity, they rely on large-scale connectivity and are fundamentally agnostic as to the function of each node. The results of such approaches are also dependent on the type of data and the methods applied. For instance, one researcher might focus on purely functional measures, such as task-based fMRI and the co-occurrence of activity across brain regions and domains; a second researcher, instead, might focus on spontaneous, resting-state activity and slow-frequency time series correlations.

As recently pointed out (5), none of these methods is guaranteed to converge and provide a functional explanation *from* the data. However, the same methods can be successfully used to test a model *against* the data via a “top-down” approach (5). That is, given a candidate functional model of the brain, traditional connectivity methods can provide reliable answers as to its degree of fidelity to the empirical data and its performance compared to other models. A top-down approach, however, critically depends on having a likely and theoretically-motivated functional proposal for a brain architecture.

The Common Model of Cognition

A promising candidate architecture is the Common Model of Cognition (CMC) (6). The CMC is an architecture for general intelligence that reflects the historical convergence of multiple computational frameworks (developed over the course of five decades in the fields of cognitive psychology, artificial intelligence, and robotics) that agree on a common set of organizing principles. The CMC assumes that agents exhibiting human-like intelligence share five functional components: A feature-based, declarative *long-term memory*, a buffer-based *working memory*, a reinforcement-learning-based set of state-action patterns represented in *procedural memory*, and dedicated *perception* and *action* systems. Working memory acts as the hub through which all of the other components communicate, with one additional connection

between perception and action (Fig. 1A). The CMC also includes a set of constraints on the mechanisms and representations that characterize each component's functional properties.

The CMC's components and assumptions distill lessons learned over the last fifty years in the development of computational cognitive models and artificial agents with general human-like abilities. Surprisingly, these lessons seem to cut across specific application domains. For instance, the cognitive architecture Soar (7) is predominantly used in designing autonomous artificial agents and robots, while the cognitive architecture ACT-R (8) is predominantly used to simulate psychological experiments and predict human behavior (9); yet, they separately converged on the CMC assumptions (6). Similarly, the SPAUN large-scale brain model (10) and the Leabra neural architecture (11) are independently designed to simulate brain function through artificial neurons, and yet they also make use of similar components and functional assumptions. Even recent AIs that are made possible by advances in artificial neural networks employ, at some level, the same components. DeepMind's AlphaGo, for example, includes a Monte Carlo search tree component for look-ahead search and planning (working memory) and a policy network (i.e., procedural memory), in addition to dedicated systems for perception and action (12). Similarly, the Differentiable Neural Computer uses supervised methods to learn optimal policies (procedural memory) to access an external memory (symbolic long-term memory) (13).

Because the CMC reflects the general organization of systems explicitly designed to achieve human-like flexibility and intelligence, the CMC should also apply to the human brain. Therefore, it provides an ideal candidate for a top-down examination of possible brain architecture.

Assuming that the CMC is a valid candidate, how can its viability as a model of the human brain architecture be assessed? Operationally, a candidate model should successfully satisfy two criteria. The first is the *generality* criterion: The same cognitive architecture should account for brain activity data across a wide spectrum of domains and tasks. The second is the *comparative superiority* criterion: An ideal architecture should provide a superior fit to experimental brain data compared to competing architectures of similar complexity.

To test the CMC against these two criteria, we conducted a comprehensive analysis of task-related neuroimaging data from 200 young adult participants in the Human Connectome Project (HCP), the largest existing repository of high-quality human neuroimaging data. Although the HCP project contains both fMRI and MEG data, fMRI was chosen because it allows for unambiguous identification of subcortical sources of brain activity, which is crucial to the CMC and problematic for MEG analysis. The HCP includes functional neuroimages collected while participants performed seven psychological tasks. These tasks were taken or adapted from previously published influential neuroimaging studies and explicitly selected to cover the range of human cognition (14), therefore making it an ideal testbed for the *generality* criterion. Specifically, the tasks examine language processing and mathematical cognition (15), working memory, incentive processing and decision making (16), emotion processing (17), social cognition (18), and relational reasoning (19). The seven tasks were collected from six different paradigms (Table S1; language processing and mathematical cognition were tested in the same paradigm).

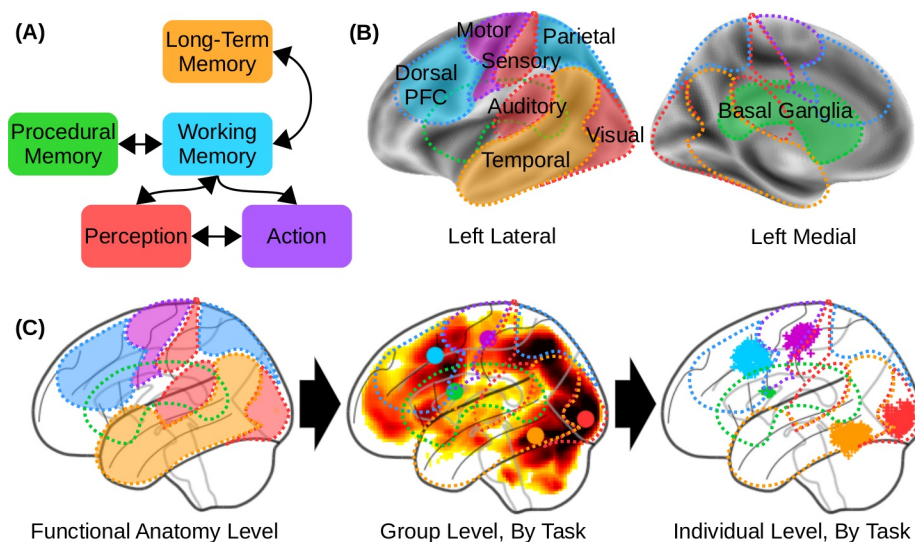


Fig. 1. The components of the Common Model of Cognition and their homologous brain regions. (A) Architecture of the Common Model of Cognition, as described in (6). (B) Theoretical mapping between CMC components and homologous cortical and subcortical regions, as used in this study's pipeline to identify the equivalent Regions of Interest (ROIs). (C) Progressive approximation of the ROIs, from high-level functional mappings (left) to task-level group results (middle, with group-level centroid coordinated marked by a color circle) to the individual functional centroids of the regions in our sample (right; each individual centroid represented by a "+" marker). Group-level and individual-level data come from the Relational Reasoning task (see Fig. 2D).

To properly translate the CMC into a brain network architecture, its five components need to be identified with an equal number of spatially-localized but functionally homologous Regions of Interest (ROIs). To objectively define these ROIs for each task and participant, a processing pipeline was set up (See Supplementary Materials for details). The starting point of the pipeline was a-priori, theoretical identification of each CMC component with large-scale neuroanatomical distinctions. This initial identification was based on well established findings in the literature, and is also consistent with the function-to-structure mappings that had been proposed in other neurocognitive architectures, such as the mappings suggested for ACT-R's module-specific buffers (8, 20, 21) or for SPAUN's component neural circuits (10).

At this level, the working memory (WM) component was identified with the fronto-parietal network comprising the dorsolateral prefrontal cortex (PFC) and posterior parietal cortex; the long-term memory (LTM) component with regions in the middle, anterior, and superior temporal lobe; the procedural knowledge component with the basal ganglia; the action component with the premotor and primary motor cortex; and perception with sensory regions, including the primary and secondary sensory and auditory cortices, and the entire ventral visual pathway, the latter of which comprises the occipital and inferior temporal lobes (Fig. 1B).

Beginning with these macro-level associations, the pipeline progressively refined the exact ROI for each component through two consecutive approximations. Fig 1C provides a visual illustration of this procedure using the data from the relational reasoning task. First, data from each task was analyzed at a group level through canonical General Linear Model (GLM) analysis, and the most functionally active focus within each macro-region was identified (Fig. 1C, middle panel; Fig. S1). This step provided reasonable neural correlates of each component for each task. Note that allowing task-based variation in the localization of each ROI implicitly makes it harder for each model to achieve the generality criterion.

The coordinates of each focus were then used as the starting point to search in 3D space for the closest active peak within the individual statistical parameter maps obtained from GLM models of each participant (see Fig. 1C, right panel). Finally, the individualized ROI coordinates were then used as the center of a spherical ROI (Table S2). Fig. 2 illustrates the distribution of the individual ROI centroids for each task, overlaid over a corresponding group-level statistical map of task-related activity. For each ROI of every participant in every task, a representative time course of neural activity was extracted as the first principal component of the time series of all of the voxels within the sphere.

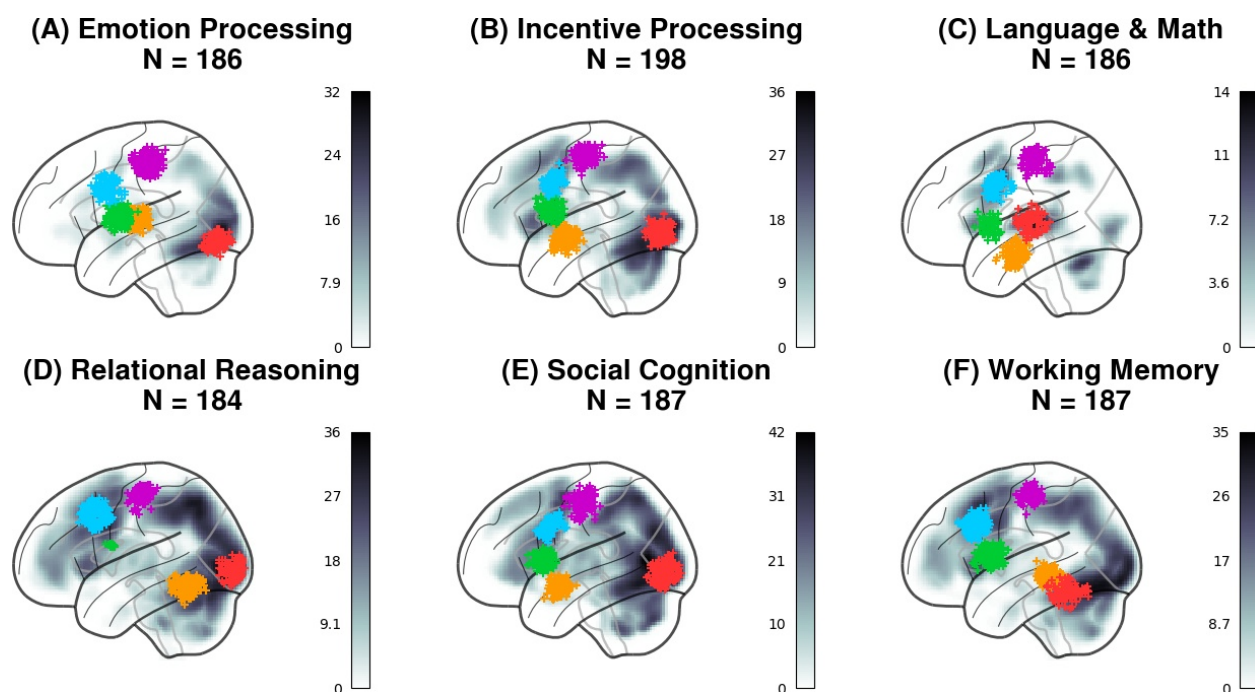


Fig. 2. Lateral view of the distribution of the ROI centroids across individual participants and tasks. Each “+” marker represents the centroid of an ROI for one participant. Colors represent the components, following the conventions of Fig 1A-C. The background represents the statistical group analysis used to identify the seed coordinate for each ROI (i.e., Step 2 in Fig. 1C).

155

All the ROIs were located in the left hemisphere; this simplifying approach was preferred to possible alternatives, such as including homologous regions in the right hemisphere (which would have required introducing additional assumptions about inter-hemispheric connectivity) or creating bi-lateral ROIs (which would have reduced the amount of variance captured in each ROI). Because all tasks show stronger activation in the left hemisphere than in the right, our results are still representative of brain activity in these domains. Finally, a network was created by connecting all the individually-defined ROIs according to the specifications of the CMC (Fig. 3A). It should be noted that synaptic pathways exist that connect every pair of components; thus, this network model is designed to capture the fundamental layout of a brain architecture in terms of functionally necessary connections, rather than anatomical details.

The link between the network of ROIs and their neural activity was provided through Dynamic Causal Modeling (DCM) (22), a neuronal-mass mathematical modeling technique that approximates the time-course of brain activity in a set of brain regions as a dynamic system that responds to a series of external drives. Specifically, the time course of the underlying neural activity y of a set of regions is controlled by the bilinear state change equation:

$$dy/dt = \mathbf{A}y + \sum_i x_i \mathbf{B}_i y + \mathbf{C}x$$

where x represents the event vectors (i.e., the equivalent of a design matrix in traditional GLM analysis), \mathbf{A} defines intrinsic connectivity between ROIs, \mathbf{C} defines the ROI-specific effects of task events, and \mathbf{B} defines the modulatory effects that task conditions have on the connectivity between regions. For simplicity, the modulatory effects in \mathbf{B} were set to zero, reducing the equation to the form $\mathbf{A}y + \mathbf{C}x$. A predicted time course of BOLD signal was then generated by applying a biologically-plausible model (the balloon model: (23, 24)) of neurovascular coupling to the simulated neural activity y . The parameters of the full DCM model were estimated by applying the expectation-maximization procedure (22) to reduce the difference between the predicted and observed time course of the BOLD signal in each ROI.

Our preference for this technique was motivated by the existence of an integrated framework to design, fit, and evaluate models; by its ability to estimate the directional effects within a network (as opposed to traditional functional connectivity analysis); and by its underlying distinction between the modeling of network dynamics and the modeling of recorded imaging signals (as opposed to Granger causality), which makes it possible to apply the same neural models to different modalities (e.g., M/EEG data) in future work.

Alternative Architectures

To address our second criterion of *comparative superiority*, the CMC dynamic model was compared against other DCM models that implement alternative brain architectures. Because the space of possible models is large, we concentrated on four models that are representative of theoretical neural architectures previously suggested in the neuroscientific literature (Fig. 3). These four models can be divided into two families. In the “Hierarchical” family, brain connectivity implements hierarchical levels of processing that initiate with Perception and

culminate with Action. In this family, the brain can be abstracted as a feedforward neural network model with large-scale gradients of abstraction (3).

Within this hierarchical structure, each ROI represents a different level and projects both forward to the next level's ROI and backwards to the preceding level's ROI. In the *open-loop* variant, Perception gives rise to two distinct branches, one feeding the LTM component (representing the abstraction of perception into memory) and one ascending to procedural memory, WM and, eventually, Action components. The second, *closed-loop* hierarchical model also incorporates bidirectional connections between LTM and WM, thus reconnecting the two pathways into a loop (Fig. 2B).

In the "Hub and Spoke" family (Fig. 2C), a single ROI is singled out as the network's "Hub" and receives bidirectional connections from all the other ROI (the "Spokes"). With the exception of the Hub, no ROI is mutually connected to any other one. In the first variant, the role of the Hub is played by the WM component. Because, in our mapping, the WM component corresponds to the lateral PFC, this model captures the increasingly popular and supported view of PFC as a flexible hub for control (2, 25). In the second variant, the role of the Hub is played by the Procedural Memory component, which reflects the centrality of procedural control in many production-system-based cognitive architectures (7, 8, 26). Because, in our mapping, Procedural Memory is identified with the basal ganglia, this architecture also reflects the centrality of these nuclei in action selection and in coordinating cortical activity (10, 27, 28).

Like the CMC, these architectures are representative of how the five components could be organized in a large-scale conceptual blueprint for the brain architecture; they simply make different choices as to which connections between components are more fundamental and better reflect the underlying neural organization. In addition to representing plausible alternative architectures, these alternative models differ minimally from the CMC and can be easily generated by replacing at most five connections from the CMC architecture (dashed lines and red lines, Fig. 2B-C). Thus, any resulting differences in fit are unlikely to arise because of differences in network complexity.

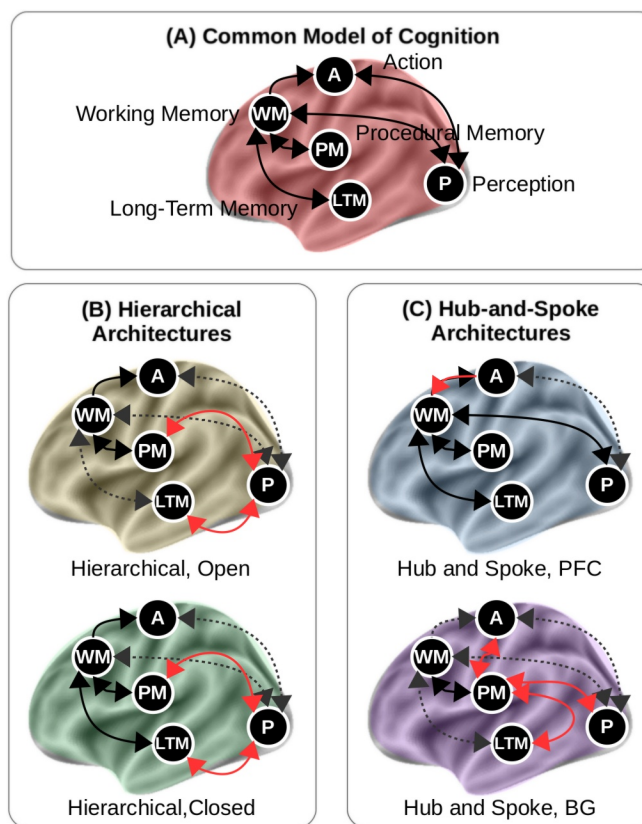


Fig 3. The five large-scale brain architectures tested in this study. (A) The CMC; (B) The “Open” and “Closed” versions of the hierarchical family; (C) The prefrontal (PFC) and basal ganglia (BG) versions of the hub-and-spoke architecture. In (B) and (C), pathways that are common to the CMC are shown in black; pathways that are present in the CMC but not included in the alternative models are shown in grey dashed arrows; and pathways that are present in the alternative models but not in the CMC are shown in red.

Once the five DCM models were separately fitted to the functional neuroimaging data, they were compared against each other using a Bayesian random-effects procedure (29). Like many other model comparison procedures, this approach provides a way to balance the complexity of a model (as the number of free parameters) versus its capacity to fit the data. Compared to popular log-likelihood-based measures (e.g., Akaike's information criterion (30)), this procedure is more robust in the face of outlier subjects, and thus better suited for studies that, like the present one, include a large number of participants and introduce considerable inter-individual variability (29, 31). (See Supplementary Materials).

Specifically, the probability r_k that a model k would fit a random individual in a sample of participants is drawn from a Dirichlet distribution $\text{Dir}(\alpha_1, \alpha_2, \dots, \alpha_K)$, and the distributions of probabilities of architectures 1, 2... k across n individuals are then drawn from multinomial distributions (see Fig. S4). The result of this modeling effort is a distribution of probabilities r_k for each model. These distributions can then be compared in terms of their relative *expected* and *exceedance* probabilities, that is, the mean probability of each model's r_k across the sample and the probability that r_k is larger than the competing models.

This procedure ultimately yields five probability distributions (one for each model), each corresponding to a specific Dirichlet value of the Dirichlet parameter α . These distributions are visualized for each task in Fig 4A-F. Furthermore they can be characterized with two metrics: the distribution's *expected* probability (i.e., the mean value of the distribution) and its *exceedance* probability (i.e., the probability that a value sampled from a distribution will exceed any value sampled from any other distribution) (29). The expected probabilities are represented as the colored vertical lines in Fig. 4A-F, while the exceedance probabilities are summarized as colored bars in Fig 4H; their exact values are listed in Table S3.

Both metrics provide evidence in favor of the CMC. As shown in Fig. 4A-F, the CMC provides a better fit to the data than any alternative architecture, and its exceedance probabilities range from 0.75 to 1.0 (Fig. 3H). Thus, the CMC uniquely satisfies both the generality and comparative superiority criteria. By contrast, all of the other architectures are consistently outperformed by the CMC in every domain (violating comparative superiority) and their relative rankings change from task to task (violating generality).

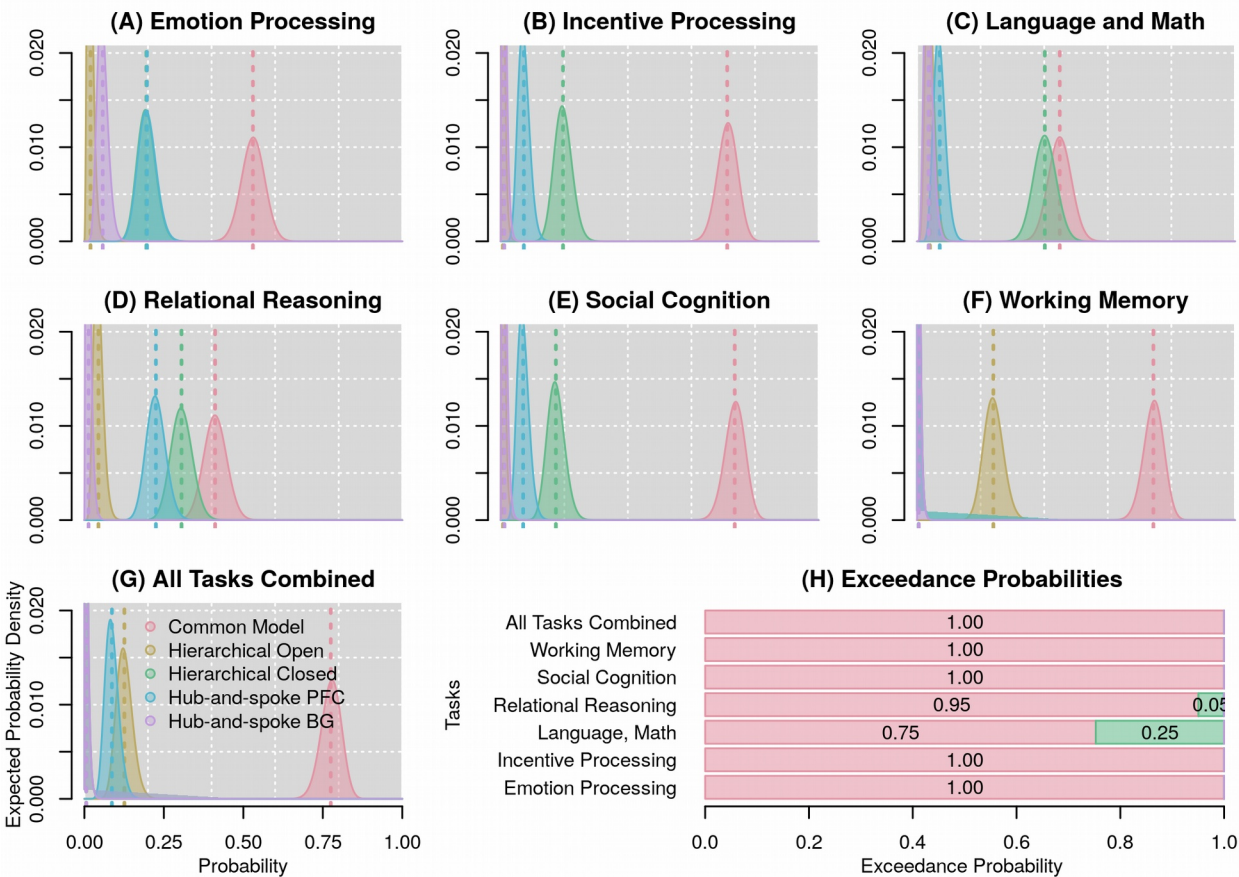


Fig 4. Results of the Bayesian model comparisons within and across tasks. In all plots, different colors represent different architectures. (A-G) Probability distributions that each of the five architectures is true, given the data within each task and across all tasks combined. Vertical dotted lines represent the mean of each distribution, i. e. the expected probability of each model. (H) Corresponding exceedance probabilities, within and across tasks, represented as stacked horizontal bars.

It is interesting to note that, across tasks, the relative ranking of the architectures does not reflect their relative similarity, measured as the number of different connections. For instance, the PFC variant of the “Hub-and-Spoke” family (Fig. 3C) is the one model most similar to the CMC, but is consistently outperformed by other models that, across all tasks, come closer to the CMC distributions (Fig. 4A-F). This fact further suggests that the CMC superiority is due to the holistic nature of its connectivity (i.e., how the components “go together”) rather than to the sum of its specific connectivity elements.

The only task in which another model comes close to the CMC in terms of fit was the Language and Mathematical cognition paradigm, in which the Hierarchical Closed model had a 0.25 exceedance probability against the CMC (Fig. 3H). This paradigm was unique because it included two entirely different tasks of comparable difficulty, instead of a single task with two conditions of different difficulty, as was the case in all other tasks. This peculiarity raises a potential concern that the CMC’s superiority could be an artifact of modeling each task in isolation, and that in conditions where multiple tasks were modeled simultaneously, a different model could potentially provide a superior fit. To examine this possibility, a second analysis was carried out, which included only the 168 participants for whom data for all seven tasks was available. In this analysis, the data from each of the six paradigms performed by the same individual is modeled as a different run from a “meta-task” performed by that individual. When such an analysis was performed, the CMC maintained its superiority, all other models having a combined exceedance probability $< 1.0 \times 10^{-10}$ (Fig. 4G-H).(32)

As noted earlier, although the competing architectures were chosen to represent current alternatives views, we cannot entirely rule out the existence of alternative architectures that explain the data better than the CMC. It is possible, however, to decide whether all of the connections in the CMC are necessary, or whether a simpler model could potentially fit the data equally well. To this end, a Bayesian parameter averaging procedure (33) was conducted to generate the posterior distributions of parameter values across participants for each task. Fig. 4 depicts the mean value (as the square color) and the associated posterior probability (as the overlaid number) for each CMC connection in each task. As the figure shows, the parameter values change significantly from task to task, implying that the CMC architecture is adaptively leveraged to meet the specific requirements of each paradigm. Nonetheless, virtually all parameters have a posterior probability $p \approx 1.0$ of being different than zero (with just two parameters having smaller probabilities, of $p = 0.75$ and $p = 0.98$), suggesting that all the components and their functional connections remain necessary across all domains.

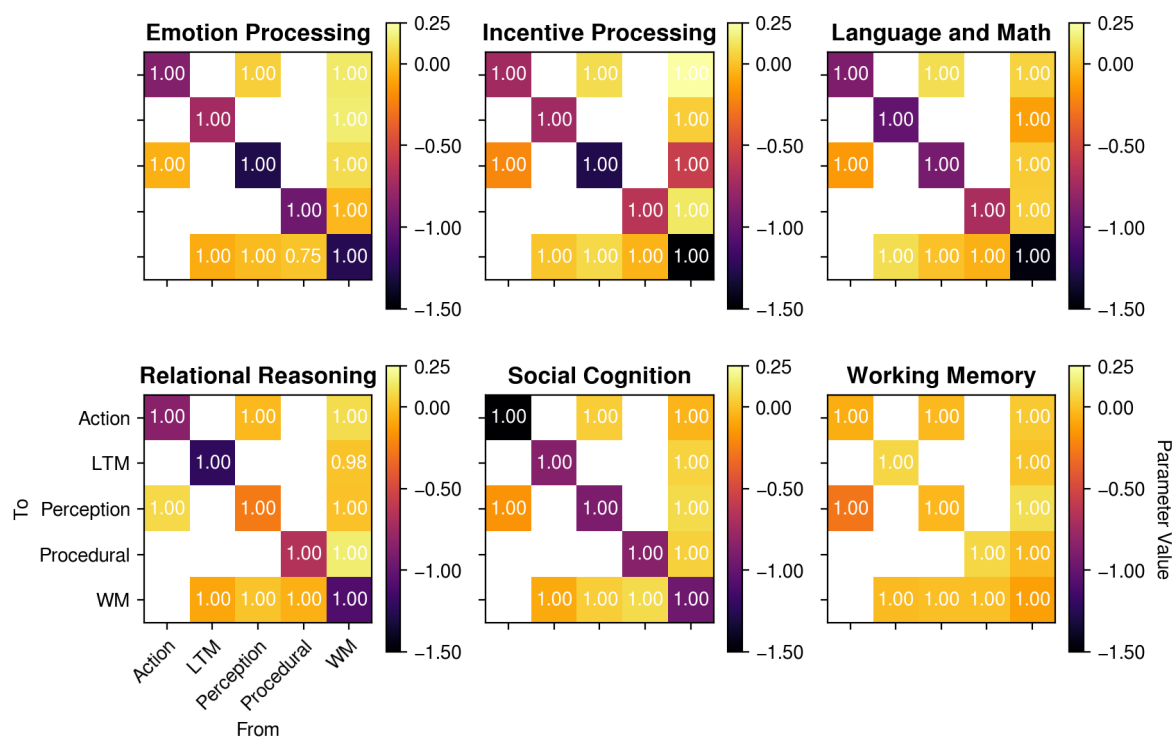


Fig. 5. Estimated DCM parameters for the CMC model cross tasks. In each plot, the color indicates the parameter value, and the white text indicates the posterior probability that the parameter value is significantly different than zero. White squares represent non-existing connections (see Fig. 1A).

310

Discussion

In summary, these results provide overwhelming and converging evidence for the CMC as a high-level blueprint of the human brain's architecture, potentially providing the missing unifying framework to relate brain structure and function for research and clinical purposes. Although surprisingly robust, these results should be considered in light of three potential limitations. First, our conclusions are based on an analysis of task-related brain activity. Despite being established in the literature, the HCP tasks remain artificial, laboratory tasks, and their ecological validity is unknown. In contrast, many prominent studies have focused on task-free, resting-state paradigms. Thus, although the use of the task-related activity provides the most natural test for the generality criterion, the extent to which the CMC applies to resting-state fMRI remains to be explored. Second, as noted above, our selection of alternative models was representative but not exhaustive. Although most distinct architectures that can be generated using just the CMC components are likely to be unreasonable from a functional standpoint, some of them could outperform the CMC. Finally, it can be argued that our approach does not take full advantage of the possibilities of DCM, which makes it possible to accommodate non-linear, modulatory effects in the dynamic model. For example, the strategic role of procedural knowledge in the CMC (Assumption B3 of the original paper) is compatible with a "modulatory" view of the basal ganglia, which has also been proposed (27) and observed (34).

These limitations notwithstanding, the fact that the CMC, which draws inspiration from high-level models of human cognition and *artificial* intelligent systems, also accounts for the neural activity of the human brain, which is a low-level *biological* intelligent system, is worthy of consideration. A mundane explanation could simply be that humans reproduce the fundamental architecture of their intelligence when designing human-like models and intelligent systems. A more radical explanation is that the architectural space for general (or, at least, human-like) intelligence is inherently constrained and possibly independent of its physical realization, whether organic or artificial. Both hypotheses are worth exploring in future research.

References and Notes

1. D. Hassabis, D. Kumaran, C. Summerfield, M. Botvinick, Neuroscience-Inspired Artificial Intelligence. *Neuron*. **95**, 245–258 (2017).
2. M. W. Cole *et al.*, Multi-task connectivity reveals flexible hubs for adaptive task control. *Nat. Neurosci.* **16**, 1348–1355 (2013).
3. J. M. Huntenburg, P.-L. Bazin, D. S. Margulies, Large-Scale Gradients in Human Cortical Organization. *Trends Cogn. Sci.* **22**, 21–31 (2018).
4. K. J. Gorgolewski *et al.*, A correspondence between individual differences in the brain's intrinsic functional architecture and the content and form of self-generated thoughts. *PLoS One*. **9**, e97176 (2014).
5. E. Jonas, K. P. Kording, Could a Neuroscientist Understand a Microprocessor? *PLoS Comput. Biol.* **13**, e1005268 (2017).

6. J. E. Laird, C. Lebiere, P. S. Rosenbloom, A Standard Model of the Mind: Toward a Common Computational Framework Across Artificial Intelligence, Cognitive Science, Neuroscience, and Robotics. *AI Magazine*. **38** (2017).
7. J. E. Laird, *The Soar Cognitive Architecture* (MIT Press, 2012).
8. J. R. Anderson, *How Can the Mind Occur in the Physical Universe?* (Oxford University Press, 2007).
9. I. Kotseruba, J. K. Tsotsos, 40 years of cognitive architectures: core cognitive abilities and practical applications. *Artificial Intelligence Review*, **40**, 1–78 (2018).
10. C. Eliasmith *et al.*, A large-scale model of the functioning brain. *Science*. **338**, 1202–1205 (2012).
11. R. C. O'Reilly, T. E. Hazy, S. A. Herd, The Leabra Cognitive Architecture: How to Play 20 Principles with Nature. *The Oxford handbook of cognitive science*, 91 (2016).
12. D. Silver *et al.*, Mastering the game of Go with deep neural networks and tree search. *Nature*. **529**, 484–489 (2016).
13. A. Graves *et al.*, Hybrid computing using a neural network with dynamic external memory. *Nature*. **538**, 471–476 (2016).
14. D. C. Van Essen *et al.*, The WU-Minn Human Connectome Project: An overview. *Neuroimage*. **80**, 62–79 (2013).
15. J. R. Binder *et al.*, Mapping anterior temporal lobe language areas with fMRI: a multicenter normative study. *Neuroimage*. **54**, 1465–1475 (2011).
16. M. R. Delgado, L. E. Nystrom, C. Fissell, D. C. Noll, J. A. Fiez, Tracking the hemodynamic responses to reward and punishment in the striatum. *J. Neurophysiol.* **84**, 3072–3077 (2000).
17. A. R. Hariri, A. Tessitore, V. S. Mattay, F. Fera, D. R. Weinberger, The amygdala response to emotional stimuli: a comparison of faces and scenes. *Neuroimage*. **17**, 317–323 (2002).
18. T. Wheatley, S. C. Milleville, A. Martin, Understanding animate agents: distinct roles for the social network and mirror system. *Psychol. Sci.* **18**, 469–474 (2007).
19. R. Smith, K. Keramatian, K. Christoff, Localizing the rostrolateral prefrontal cortex at the individual level. *Neuroimage*. **36**, 1387–1396 (2007).
20. J. P. Borst, M. Nijboer, N. A. Taatgen, H. van Rijn, J. R. Anderson, Using data-driven model-brain mappings to constrain formal models of cognition. *PLoS One*. **10**, e0119673 (2015).
21. J. P. Borst, J. R. Anderson, Using model-based functional MRI to locate working memory updates and declarative memory retrievals in the fronto-parietal network. *Proc. Natl. Acad. Sci. U. S. A.* **110**, 1628–1633 (2013).
22. K. J. Friston, L. Harrison, W. Penny, Dynamic causal modelling. *Neuroimage*. **19**, 1273–1302 (2003).
23. K. J. Friston, A. Mechelli, R. Turner, C. J. Price, Nonlinear responses in fMRI: the Balloon model, Volterra kernels, and other hemodynamics. *Neuroimage*. **12**, 466–477 (2000).

24. R. B. Buxton, E. C. Wong, L. R. Frank, Dynamics of blood flow and oxygenation changes during brain activation: the balloon model. *Magn. Reson. Med.* **39**, 855–864 (1998).
- 390 25. M. W. Cole, T. Yarkoni, G. Repovs, A. Anticevic, T. S. Braver, Global connectivity of prefrontal cortex predicts cognitive control and intelligence. *J. Neurosci.* **32**, 8988–8999 (2012).
- 395 26. D. E. Kieras, D. E. Meyer, An overview of the EPIC architecture for cognition and performance with application to human-computer interaction. *Human-computer interaction.* **12**, 391–438 (1997).
27. A. Stocco, C. Lebiere, J. R. Anderson, Conditional routing of information to the cortex: A model of the basal ganglia's role in cognitive coordination. *Psychol. Rev.* **117**, 540–574 (2010).
- 400 28. T. E. Hazy, M. J. Frank, R. C. O'reilly, Towards an executive without a homunculus: computational models of the prefrontal cortex/basal ganglia system. *Philos. Trans. R. Soc. Lond. B Biol. Sci.* **362**, 1601–1613 (2007).
29. K. E. Stephan, W. D. Penny, J. Daunizeau, R. J. Moran, K. J. Friston, Bayesian model selection for group studies. *Neuroimage.* **46**, 1004–1017 (2009).
- 405 30. H. Akaike, in *Selected Papers of Hirotugu Akaike* (Springer, 1974), pp. 215–222.
31. K. E. Stephan *et al.*, Ten simple rules for dynamic causal modeling. *Neuroimage.* **49**, 3099–3109 (2010).
32. C. H. Kasess *et al.*, Multi-subject analyses with dynamic causal modeling. *Neuroimage.* **49**, 3065–3074 (2010).
- 410 33. C. S. Prat, A. Stocco, E. Neuhaus, N. M. Kleinhaus, Basal ganglia impairments in autism spectrum disorder are related to abnormal signal gating to prefrontal cortex. *Neuropsychologia.* **91**, 268–281 (2016).
34. D. M. Barch *et al.*, Function in the human connectome: task-fMRI and individual differences in behavior. *Neuroimage.* **80**, 169–189 (2013).
- 415 35. R. L. Buckner, F. M. Krienen, A. Castellanos, J. C. Diaz, B. T. T. Yeo, The organization of the human cerebellum estimated by intrinsic functional connectivity. *J. Neurophysiol.* **106**, 2322–2345 (2011).
36. F. Castelli, F. Happé, U. Frith, C. Frith, Movement and mind: a functional imaging study of perception and interpretation of complex intentional movement patterns. *Neuroimage.* **12**, 314–325 (2000).
- 420 37. W. D. Penny, K. J. Friston, J. T. Ashburner, S. J. Kiebel, T. E. Nichols, *Statistical Parametric Mapping: The Analysis of Functional Brain Images* (Academic Press, 2011).
38. J. Ashburner *et al.*, SPM12 manual. Available at:
http://www.fil.ion.ucl.ac.uk/spm/doc/spm12_manual.pdf
- 425 39. G. Schwarz, Estimating the Dimension of a Model. *Ann. Stat.* **6**, 461–464 (1978).

Acknowledgments

The authors would like to thank Jim Treyens and John R. Anderson for their comments on early drafts of this manuscript. **Funding:** This effort has been sponsored by award FA9550-19-1-0299 from the Air Force Office of Scientific Research (AFOSR) to AS, by award FA9550-19-0180 from AFOSR to JL, by award W911NF-14-D-0005 from the U. S. Army to PR, and by an award from the Defense Advanced Research Projects Agency (DARPA) to CL. Statements and opinions expressed do not necessarily reflect the position or the policy of the United States Government, and no official endorsement should be inferred. **Author contributions:** Conceptualization: AS, CL, JL, and PR; Data curation: AS, NK, and ZSH; Formal analysis: AS, NK, and ZSH; Funding acquisition AS, CL, JL, and PR; Investigation: AS, CL, JL, and PR; Methodology: AS; Project administration: AS; Resources AS, CL, JL, and PR; Software: AS, NK and ZSH; Visualization: AS; Writing: AS, CL, JL, NK, PR and ZSH. **Competing interests:** The authors declare no competing interests; and **Data and materials availability:** All the raw imaging data is available through the Human Connectome Project (<http://www.humanconnectome.org>). All the pipeline scripts designed to preprocess the data, generate and fit the DCM models, extract and interpret the results, and generate the figures reported in this paper are available as an open-source code repository on <https://github.com/UWCCDL/CMC-DCM>.

Supplementary Materials:

Materials and Methods

Figures S1-S4

Tables S1-S3

References (None).